

Downstream flow condition effects on the RR → MR transition of asymmetric shock waves in steady flows

Z. M. HU, R. S. MYONG[†], M. S. KIM AND T. H. CHO

Research Center for Aircraft Parts Technology and School of Mechanical and Aerospace Engineering,
Gyeongsang National University, Jinju 660-701, South Korea

(Received 25 March 2008 and in revised form 3 September 2008)

In this paper, the regular reflection (RR) to Mach reflection (MR) transition of asymmetric shock waves is theoretically studied by employing the classical two- and three-shock theories. Computations are conducted to evaluate the effects of expansion fans, which are inherent flow structures in asymmetric reflection of shock waves, on the RR → MR transition. Comparison shows good agreement among the theoretical, numerical and experimental results. Some discrepancies between experiment and theory reported in previous studies are also explained based on the present theoretical analysis. The advanced RR → MR transition triggered by a transverse wave is also discussed for the interaction of a hypersonic flow and a double-wedge-like geometry.

1. Introduction

It is well known that for shock wave reflection in a steady flow at a sufficiently high Mach number, more than one global solution is compatible with the conservation laws and the applied boundary conditions. This leads to what is known as the dual solution. In the dual-solution domain, both regular and Mach reflection patterns (denoted by RR and MR) are locally stable for a given time history, as shown in figure 1. Intensive analytical, experimental and numerical investigations have contributed much to the understanding of the physics underlining shock wave reflection in the last few decades. The reflection phenomena of shock waves in steady, pseudo-steady and unsteady flows were summarized by Ben-Dor (1991). Shock polars for two-dimensional shock wave interactions are bounded and not monotonic, which may, consequently, have no intersection or more than one intersection in the graphical construction. When no intersection exists, the problem of non-existence is resolved with more complex wave patterns: either with transonic curved shocks or with composite wave patterns. The wave patterns of the former are not steady but may be pseudo-steady. Composite wave patterns, including single-Mach reflection, transitional-Mach reflection and double-Mach reflection, consist of multiple simple nodes separated by smoothly varying flows (see Henderson 1990; Henderson, Colella & Puckett 1991; Henderson & Menikoff 1998). In these cases, the time-dependent boundary conditions or downstream boundary conditions can cause a wave pattern to bifurcate or change the form. Bifurcations can be triggered by acoustic waves impacting a node or can be forced by a sudden change in geometry. The state of the

[†] Email address for correspondence: Email address for correspondence: myong@gnu.ac.kr

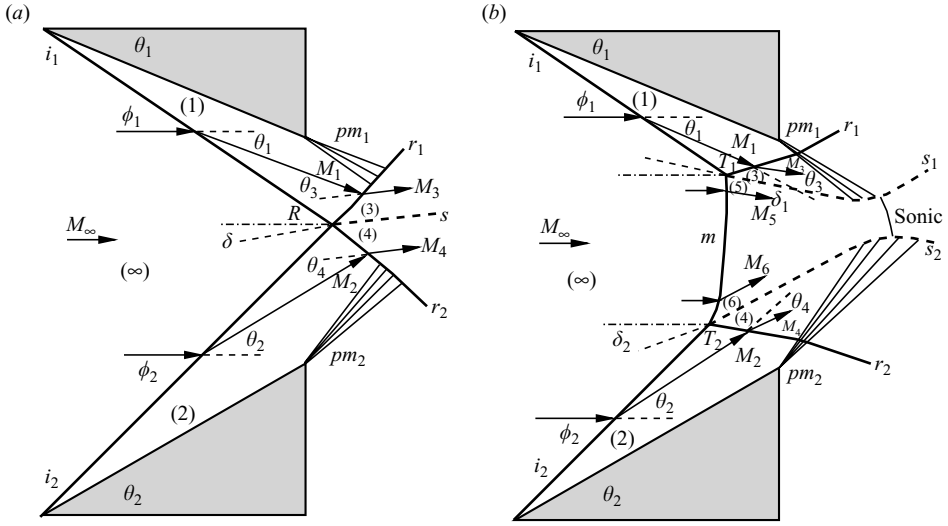


FIGURE 1. Schematic illustration of (a) an overall RR wave configuration and (b) an overall MR wave configuration in steady flows.

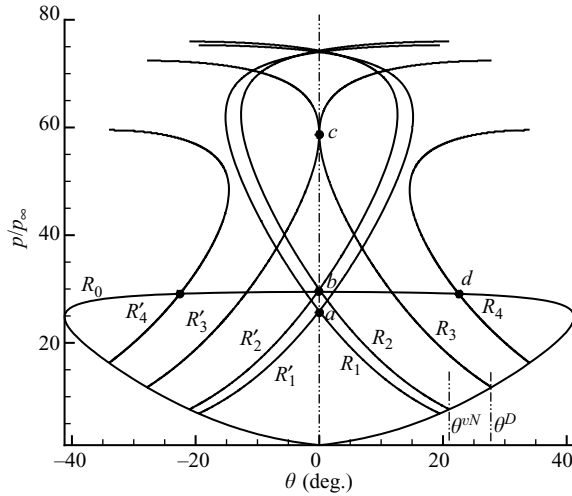


FIGURE 2. Pressure-deflection polars illustrating various theoretically admissible solutions in the reflection of symmetric shock waves in steady flows.

knowledge in this research field was demonstrated by Ben-Dor (1991) and was then reviewed by Ben-Dor (2006).

It was von Neumann (1943) who first introduced the criteria for the RR ↔ MR transitions. The criteria are given by the detachment condition, beyond which RR wave configuration is theoretically inadmissible, and by the von Neumann condition, beyond which MR configuration is theoretically inadmissible. Both RR and MR wave configurations are theoretically admissible inside the parameter space bounded by these two conditions. Figure 2 schematically shows the transition criteria for the interaction of shock waves of opposite families generated by two symmetrically arranged wedges or for reflection of a single shock wave over a horizontal plate. In figure 2, points *b* and *c* correspond to the von Neumann condition and the

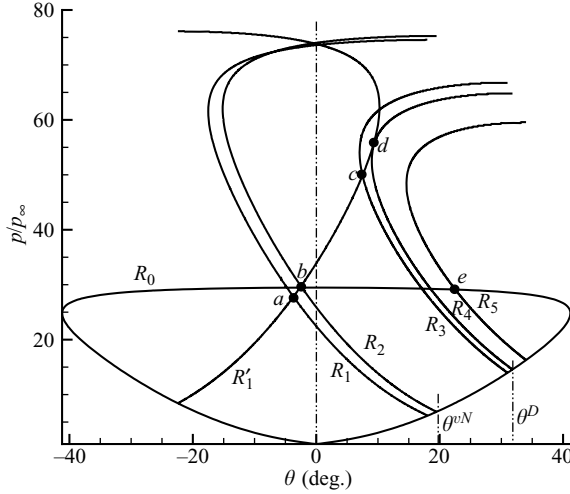


FIGURE 3. Pressure-deflection polars illustrating various theoretically admissible solutions in the reflection of asymmetric shock waves in steady flows (according to the detachment and the von Neumann criteria hypothesized by Li *et al.* 1999).

detachment condition, respectively, while points *a* and *d* denote an overall RR solution and an overall MR solution, respectively. Hornung, Oertel & Sandeman (1979) first hypothesized that hysteresis could be present during the RR ↔ MR transition process. With increasing wedge angle the RR → MR transition occurs near the detachment condition, while with decreasing wedge angle the MR → RR transition occurs at the von Neumann condition. The hysteresis phenomenon has been proved by experiments (see Chpoun, Passerel, Li & Ben-Dor 1995; Skews 1997, 2000; Li, Chpoun & Ben-Dor 1999; Ivanov *et al.* 2001; Sudani *et al.* 2002) and computations (see Chpoun & Ben-Dor 1995; Vuillon, Zeitoun & Ben-Dor 1995; Ivanov *et al.* 1996, 2002; Henderson, Crutchfield & Virgona 1997; Ben-Dor, Elperin & Vasilev 1999; Kudryavtsev *et al.* 2002). Ben-Dor *et al.* (2002) reviewed the hysteresis process.

As shown in figure 1(*a*), an overall RR wave pattern consists of two incident shock waves (i_1 and i_2), two reflected shock waves (r_1 and r_2), one slipstream (s) and two Prandtl–Meyer expansion fans (pm_1 and pm_2). These discontinuities excluding pm_1 and pm_2 meet at a single node (R). The boundary condition for an overall RR is

$$\theta_1 - \theta_3 = \theta_2 - \theta_4 = \delta, \quad (1.1)$$

where $\theta_1, \theta_2, \theta_3$ and θ_4 are the flow deflection angles across i_1, i_2, r_1 and r_2 , respectively. As symmetric reflection with $\theta_1 = \theta_2 = \theta_3 = \theta_4, \delta = 0$ causes the slipstream to disappear. An overall MR wave pattern, as shown in figure 1(*b*), is more complicated than an overall RR wave pattern. A Mach stem (m) bridges two triple points, T_1 connecting i_1, r_1 and s_1 and T_2 connecting i_2, r_2 and s_2 . The boundary conditions for an overall MR are

$$\theta_1 - \theta_3 = \delta_1, \theta_2 - \theta_4 = \delta_2. \quad (1.2)$$

When $\theta_1 = \theta_2$, the reflection is symmetric with $\delta_1 = \delta_2$.

Supported by analytical and experimental results, Li *et al.* (1999) proposed the corresponding transition criteria for the reflection of asymmetric shock waves. As shown in figure 3, the points *b* and *d* respectively correspond to the von Neumann

condition and the detachment condition. Hysteresis occurs between b and d during the $RR \leftrightarrow MR$ transition. Several different wave patterns that are theoretically impossible in a symmetric reflection were illustrated in their analytical work (see Li *et al.* 1999). First, one of the RRs in an overall RR wave configuration (oRR (wRR + sRR)) is theoretically admissible as a strong solution. Secondly, it is theoretically possible that one of the MRs in an overall MR wave configuration (notated as oMR (InMR + DiMR)) is an inverse MR (InMR, denoted as the wave pattern of a degenerate cross node by Henderson *et al.* 1991 and Henderson & Menikoff 1998). However, an oMR is theoretically admissible if and only if the two slipstreams assemble an overall converging stream tube. An oMR (InMR + DiMR) configuration was first experimentally demonstrated by Li *et al.* (1999). Here, wRR, sRR and DiMR denote weak RR, strong RR and direct MR, respectively.

There are two Prandtl–Meyer expansion fans (pm_1 and pm_2) emanating from the trailing edges, as shown in figure 1(a, b), respectively. They are necessary to let the locally subsonic flow downstream of the reflection point of an oRR (wRR + sRR) configuration or the Mach stem of an oMR configuration match the overall supersonic flow conditions. For example pm_1 and pm_2 reach and change the direction of slipstreams s_1 and s_2 to form a converging–diverging stream tube as shown in figure 1(b). It should be noted that the boundary condition given by (1.2) is insufficient for a stable MR configuration, and another necessary condition is a converging–diverging stream tube following the Mach stem m . Clearly, the Prandtl–Meyer expansion fans play an important role in the configuration of the asymmetric shock wave reflection through the converging–diverging stream structure. It has been shown that disturbances in the free stream flow (see Kudryavtsev *et al.* 2002) and the three-dimensional nature of the flow field can have a major effect on the transition (see Skews 1997, 2000). In addition, the numerical work of Ben-Dor *et al.* (1999) considered the effects of the downstream pressure in the wake flow of the wedge. The agreement between the experimental and analytical results concerning $RR \rightarrow MR$ transition angles is surprisingly good according to the study of Li *et al.* (1999). In contrast, the experimental $RR \rightarrow MR$ transition angles are approximately 2.5° lower than the detachment criterion in Sudani *et al.* (2002). Sudani *et al.* (2002) assumed that three-dimensional effects in the experiments of Li *et al.* (1999) delay the $RR \rightarrow MR$ transition. In fact, different translational or rotational mechanisms of the wedges were used in their experimental set-ups. As a consequence, the different movement of the expansion fans might be an additional cause for the reported discrepancy. Dynamic effects due to the transient motion or rotation of the wedges can make the transition angle slightly different from the theoretical criteria (see Mouton & Hornung 2007; Naidoo & Skews 2007). However, the fundamental physics behind the dynamic effects hasn't been well explained.

Both the RR and the MR wave configurations are stable in the dual-solution domain based on the principle of minimum entropy production (see Li & Ben-Dor 1996). On the other hand, the triple-shock theorem implies that the Mach configuration contains higher entropy compared to that of the RR. Based on thermodynamic stability, a higher entropy configuration would be preferred for a continuous transition. This provides heuristic motivation for the von Neumann point as the $MR \rightarrow RR$ transition criterion (see Henderson *et al.* 1991). Hornung (1997) and Sudani & Hornung (1998) presented an alternative means for stability analysis of RR and MR wave configurations and reached the same conclusion as Li & Ben-Dor (1996). Sudani & Hornung (1998) proposed a minimum disturbance criterion for the $RR \rightarrow MR$ transition, using an analogy based on the potential energy of a particle on

a surface, which was earlier than the detachment criterion of Li *et al.* (1999). The two criteria are identical for a symmetric shock reflection but different for an asymmetric reflection.

It is interesting to note that the motivation of studying the hysteresis phenomenon in the transition between RR and MR were purely academic. However, it was eventually found that the existence of the hysteresis process has a critical impact on the performance of the supersonic intake in an air-breathing propulsion system. Compared with the analytical study of Li *et al.* (1999), the RR \rightarrow MR transition for the reflection of asymmetric shock waves is further discussed by applying the classical two- and three-shock theories of von Neumann (1943) in the present study. Computations are conducted to evaluate the effects of the expansion fans and downstream flow conditions on the RR \rightarrow MR transition. Theoretical and numerical analyses are further performed to understand the physics behind the discrepancies reported in previous studies.

2. Shock polar analysis

It is useful to present shock interactions, using pressure-deflection polar diagrams, in which the pressure jump across a shock wave is plotted against the flow deflection angle. Briefly, the shock polar represents the locus of all flow states that can be obtained by passing through any oblique shock for a given flow Mach number. The entire region behind a planar shock wave is then represented by a single point on a (p - θ) diagram. The maximum angle that a flow can be turned by an oblique shock is easily seen: this is the point of maximum deflection that separates the polar into weak and strong regions. Just below this point on the shock polar is the sonic point. Above the sonic point are solutions that produce a subsonic flow behind the oblique shock, and below this point lie solutions that produce a supersonic flow behind the oblique shock wave. In cases with curved shock waves, the shock polar is correct only in a vanishingly small region about the interaction point.

In figure 3, the shock polar combination represents the process of the RR \leftrightarrow MR transition and the hysteresis phenomena according to the wedge assembly shown in figure 1. Also in figure 3, R_0 and R'_1 correspond to shock waves in the free stream flow and the upper reflected shock r_1 , respectively. The sequential polars R_1 to R_5 correspond to r_2 as θ_2 increases. In the RR \rightarrow MR transition process, there is a critical wedge angle $\theta_2 = \theta_2^S$ at which the loci intersect at the sonic point on the shock polar of R_5 , as shown in figure 4(a). Beyond θ_2^S the flow behind the reflected shock wave r_2 becomes locally subsonic. This wave configuration is sensitive to disturbances either in the free stream flow or from the downstream flow field and is likely to cause an RR \rightarrow MR transition. Hereafter, this critical condition is hypothesized as the sonic-point criterion for the RR \rightarrow MR transition of the reflection of asymmetric shock waves. However, a subsonic RR wave configuration may be admissible due the upstream influence of the expansion waves slightly downstream of the reflection point. It can be maintained until $\theta_2 = \theta_2^{MD}$ at which angle the flows behind both reflected shock waves r_1 and r_2 reach their maximum-deflection conditions. This special RR wave configuration features the curvature of reflected shock waves and the smooth variation of flow parameters in the zone surrounded by the reflected shock waves and expansion waves. Below θ_2^{MD} , the loci of flow Mach number intersect as shown by dashed lines in figure 4. It implies an identical flow deflection for both (3) and (4) zones (see the labels in figure 1a). In other words, the flows on both sides of the slip layer are parallel to each other. Hereafter, this critical condition at the angle θ_2^{MD} is

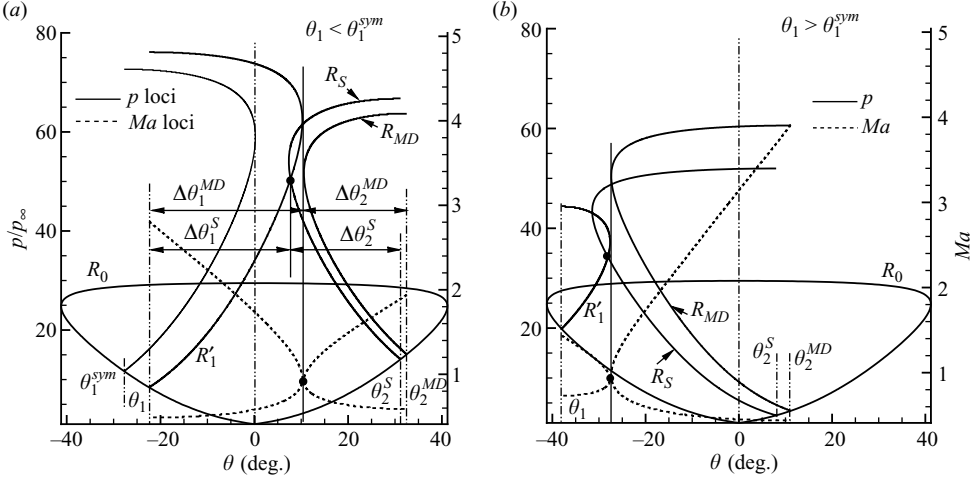


FIGURE 4. Different criteria for the RR \rightarrow MR transition: (a) $\theta_1 < \theta_1^{sym}$; (b) $\theta_1 > \theta_1^{sym}$. (R_S corresponds to the sonic-point criterion; R_{MD} corresponds to the maximum-deflection criterion; the symmetric condition refers to a certain wedge angle θ_1^{sym} , at which the sonic point of the reflected shock polar lies on the symmetry line of the polar for the free stream flow).

hypothesized as the maximum-deflection criterion for the RR \rightarrow MR transition of the reflection of asymmetric shock waves. Computations will be conducted in the next section to confirm and explain the existence of these RR wave configurations which are theoretically impossible inside the parameter domain of $(\theta_2^D, \theta_2^{MD})$. Obviously, $\theta_2^S < \theta_2^D < \theta_2^{MD}$. It is important to note that the required sonic point that determines the above-mentioned sonic-point criterion switches to the sonic point of the r_1 polar (R'_1) when $\theta_1 > \theta_1^{sym}$ as shown in figure 4(b). Here, θ_1^{sym} corresponds to a critical value of θ_1 at which the sonic point of the reflected shock polar lies on the symmetry line of the polar for the free stream flow.

The flow deflection angle θ and the pressure ratio ξ across an oblique shock wave can be related to the Mach number M ahead of the shock wave and the shock angle ϕ (see Han & Yin 1993), respectively, as follows:

$$\theta = f(\gamma, M, \phi) = \tan^{-1} \left\{ \frac{2 \cot \phi (M^2 \sin^2 \phi - 1)}{M^2 (\cos 2\phi + \gamma) + 2} \right\}, \quad (2.1)$$

$$\xi = g(\gamma, M, \phi) = 1 + \frac{2\gamma}{\gamma + 1} (M^2 \sin^2 \phi - 1). \quad (2.2)$$

Here, γ is the ratio of specific heat capacities, and the shock angle $\sin^{-1}(1/M) \leq \phi \leq \pi/2$. The maximum-deflection criterion for the RR \rightarrow MR transition shown in figure 4 can be mathematically expressed as

$$\Delta\theta_1^{MD} + \Delta\theta_2^{MD} = \theta_1 + \theta_2^{MD}, \quad (2.3)$$

where the maximum-deflection angle of the M_j ($j=1$ and 2 for the upper and the lower reflections, respectively) shock polar can be obtained by

$$\Delta\theta_j^{MD} = f(\gamma, M_j, \phi), \sin^{-1} \left(\frac{1}{M_j} \right) \leq \phi \leq \frac{\pi}{2}. \quad (2.4)$$

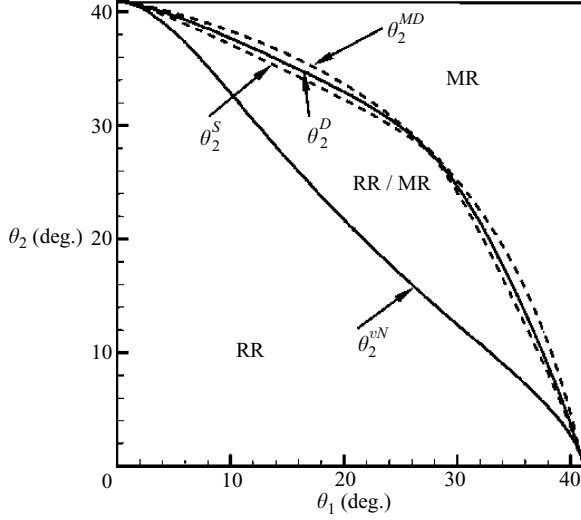


FIGURE 5. The RR ↔ MR transition criteria in the (θ_1, θ_2) plane for $M_\infty = 4.96$: the solid lines correspond to the detachment and the von Neumann criteria hypothesized by Li *et al.* (1999); the dashed lines correspond to the sonic-point and the maximum-deflection criteria.

Here, based on the basic shock wave relations, M_j is given by

$$M_j = h(\gamma, M_\infty, \phi_j) = \left\{ \frac{M_\infty^2 + \frac{2}{\gamma-1}}{\frac{2\gamma}{\gamma-1} M_\infty^2 \sin^2 \phi_j - 1} + \frac{M_\infty^2 \cos^2 \phi_j}{\frac{\gamma-1}{2} M_\infty^2 \sin^2 \phi_j + 1} \right\}^{\frac{1}{2}}. \quad (2.5)$$

For a given angle θ_1, θ_2^{MD} that satisfies the maximum-deflection criterion for RR → MR transition can be obtained from (2.3), using an iterative process.

Similarly, the sonic-point criterion for the RR → MR transition shown in figure 4 can be theoretically expressed as

$$\xi_1^0 \xi_1^S = \xi_2^0 \xi_2^S, \quad (2.6)$$

$$\Delta\theta_1^S + \Delta\theta_2^S = \theta_1 + \theta_2^S, \quad (2.7)$$

where $\xi_j^0 = g(\gamma, M_\infty, \phi_j)$ and $\xi_j^S = g(\gamma, M_j, \phi_j^S)$. Here, $j = 1$ and 2 ; the superscript '0' corresponds to the free stream flow; and 'S' denotes the sonic point of a shock polar. Again, for a given angle θ_1, θ_2^S satisfying the sonic-point criterion for the RR → MR transition can be uniquely defined by iteratively solving (2.6) and (2.7). It is important to note again that the sonic point of a shock polar, as clearly indicated by the graphical construction in figure 4(a, b), is on the R_1' shock polar when $\theta_1 > \theta_1^{sym}$, while it should be located upon the R_S shock polar when $\theta_1 < \theta_1^{sym}$.

The RR → MR transition curves for the maximum-deflection criterion given by (2.3) and the sonic-point criterion given by (2.6) and (2.7) are drawn as dashed lines in figure 5 in the (θ_1, θ_2) plane for $M_\infty = 4.96$. For a direct comparison, the detachment line (a tangent-point criterion) and von Neumann line are given as solid lines in the same figure. The details of the detachment criterion for the RR → MR transition and the von Neumann criterion for the MR → RR transition associated with asymmetric shock reflections can be found in §2.3 of Li *et al.* (1999). It can be observed in figure 5 that in the vicinity of the symmetric condition in which $\theta_1^{sym} = 27.7^\circ$ and at the zero and maximum-deflection angles, the differences among above-mentioned RR → MR transition criteria are negligible. However, significant discrepancy exists over the rest

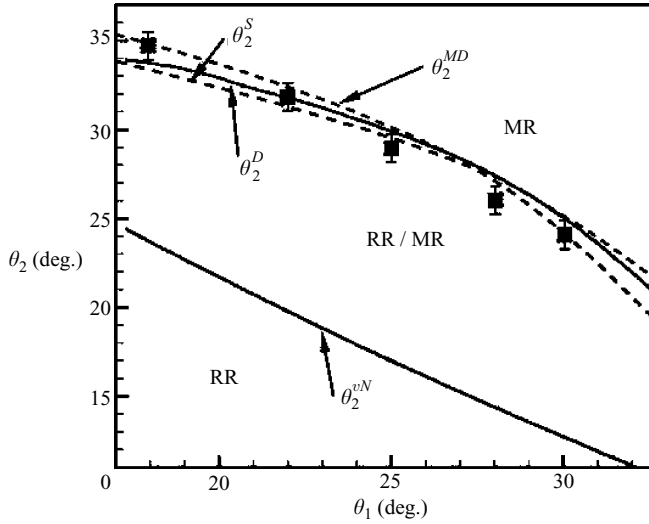


FIGURE 6. Comparison among the analytical RR \rightarrow MR transition lines and experiments in the (θ_1, θ_2) -plane for $M_\infty = 4.96$. The dashed lines correspond to the sonic-point and the maximum-deflection criteria; the solid lines correspond to the detachment and von Neumann criteria hypothesized by Li *et al.* (1999); and the solid squares are their experimentally recorded RR \rightarrow MR transition points (see Li *et al.* 1999).

of the parameter domain. It is clearly demonstrated that the RR \rightarrow MR transition line of the detachment (tangent-point) criterion lies between the maximum-deflection and the sonic-point criteria.

Comparisons among the above-mentioned RR \rightarrow MR transition lines and the experiments for the $M_\infty = 4.96$ flow in the (θ_1, θ_2) plane are shown in figure 6. The experimental data are extracted from the figure 9 of Li *et al.* (1999) and denoted here using the same symbols as in the original. Most of the experimental points associated with the RR \rightarrow MR transition scatter in the parameter domain bounded by the transition lines of the maximum-deflection and the sonic-point criteria in figure 6. Therefore, the maximum-deflection and the sonic-point criteria can explain the discrepancy between the experimental points and the transition line of the detachment criterion.

It is interesting to note that the disagreement between the experiments and the analytically predicted RR \rightarrow MR transition angles appears relatively more significant in the vicinity of the symmetry condition, i.e. $\theta_1^{sym} = 27.7^\circ$ for the $M_\infty = 4.96$ flow. It becomes apparent when referring to the concept of the threshold $\Delta p = p_{\theta_{max}} - p_{sonic}$ (see Henderson 1990; Henderson & Menikoff 1998). As shown in figure 7, the method of calculating Δp in the present investigation depends on the value of θ_1 as the sonic point, for the sonic-point transition criterion is located on the R'_1 shock polar when $\theta_1 > \theta_1^{sym}$ and switches to the R_2^S shock polar when $\theta_1 < \theta_1^{sym}$. If the magnitude of any disturbance in the flow field exceeds Δp , the RR \rightarrow MR transition can be triggered below the theoretical criterion. The solid lines in figure 8 represent the threshold in the $(\theta_1 - \Delta p)$ parameter domain for the RR \rightarrow MR transition of asymmetric shock waves for $M_\infty = 4.96$ and $M_\infty = 4.015$ flows. From the figure it can be found that the closer to the symmetric condition a polar is, the smaller Δp becomes. Therefore, in the vicinity of θ_1^{sym} , the RR wave configuration is relatively more sensitive to disturbance and consequently more likely to advance the transition into an MR configuration.

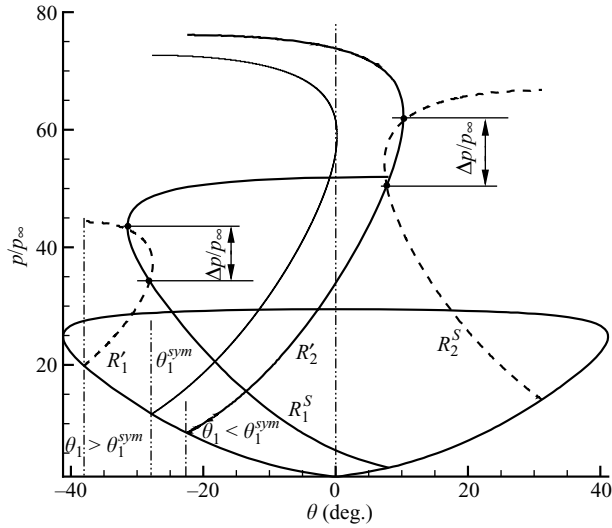


FIGURE 7. The threshold in terms of pressure difference for the RR → MR transition of asymmetric shock waves of opposite families.

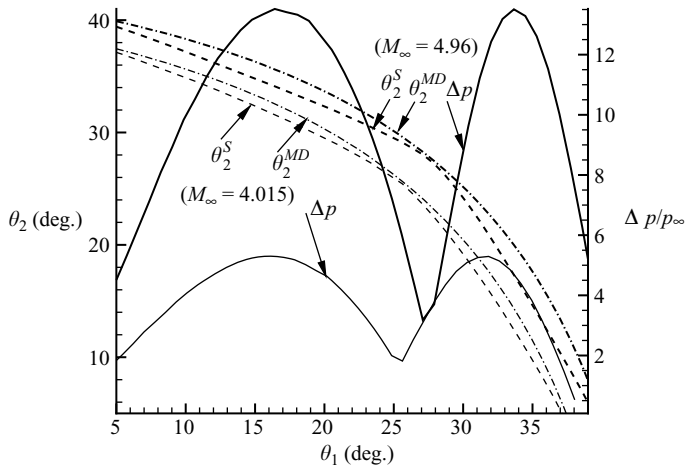


FIGURE 8. The threshold in terms of pressure difference for the RR → MR transition of asymmetric shock waves of opposite families: the thick solid line corresponds to the $M_\infty = 4.96$ flow; the thin solid line corresponds to the $M_\infty = 4.015$ flow; the dashed and the dashed-dotted lines are for the transition line of the sonic-point and the maximum-deflection criteria.

This conclusion appears to be consistent with the experimental results of Li *et al.* (1999). On the other hand, the fact that the experimental RR → MR transition angle at $\theta_1 = 18^\circ$ is beyond the θ_2^D line and very close to the θ_2^{MD} line can also prove the above conclusion. Another instance is that the RR → MR transition angles for symmetric reflections are approximately 2.1° lower than the theoretical detachment criterion (see Chpoun *et al.* 1995), which has been ascribed to three-dimensional effects and perturbation in the wind tunnels (see Chpoun *et al.* 1995; Sudani *et al.* 2002). However, it was noted that three-dimensional effects by themselves are not sufficient to promote hysteresis and that the type of the wind tunnel has a significant, and unfortunately not yet understood, influence on the occurrence of hysteresis for

RR \leftrightarrow MR transitions in steady flows (see Ben-Dor *et al.* 2002). Based upon the present analysis, the relatively smaller threshold for the RR \rightarrow MR transition in the vicinity of the symmetry condition may be an additional reason for the earlier RR \rightarrow MR transition in the presence of the noise inherent in supersonic test flows. The fact that better agreement between experimental and theoretical results for asymmetric reflections was achieved with the same facility as that of Li *et al.* (1999) supports this conclusion. It can also be found from figure 8 that the smaller the Mach number of the free stream flow, the smaller the threshold. This might be an additional cause of the earlier RR \rightarrow MR transition reported by Sudani *et al.* (2002) in which the flow Mach number $M_\infty = 4.015$ is less than that used in the experiments of Li *et al.* (1999).

The analysis in this section can be summarized as follows: The theoretical RR \rightarrow MR transition angle for an asymmetric shock wave reflection lies inside the parameter domain bounded by the sonic-point criterion line and the maximum-deflection criterion line. However, in the vicinity of the symmetric reflection condition, the RR \rightarrow MR transition is likely advanced by disturbance from the free stream or downstream flow field. If the reflection condition is away from the symmetry condition and reaches a maximum threshold, the RR \rightarrow MR transition angle is determined mainly by the maximum-deflection criterion. In the coming section, computations are conducted to verify the above hypothesis and the analytical results.

3. Numerical study

It was noted that the MR \rightarrow RR transition angle is strongly dependent on the grid size in the vicinity of the reflection point (see Ivanov *et al.* 2002; Sudani *et al.* 2002) in computations. On the other hand, the RR \rightarrow MR transition angle does not depend on the grid resolution assuming sufficient grid density but strongly depends on the numerical dissipation inherent in any shock-capturing scheme (see Ivanov *et al.* 1998; Chpoun & Ben-Dor 1995; Ben-Dor *et al.* 2002). In the following sections, only the RR \rightarrow MR transition will be numerically simulated according to the transition analysis mentioned in the previous section. For numerical algorithms in the present study, Euler equations for a perfect gas with $\gamma = 1.4$ are discretized using the second-order dispersion-controlled dissipative (DCD) scheme proposed by Jiang, Takayama & Chen (1995) and reviewed by Jiang (2004). The principle of DCD scheme aims at removing non-physical oscillation across strong discontinuities by making use of the dispersion characteristics of the modified equation instead of adding artificial viscosity. A third-order Runge–Kutta scheme is used for time integration.

The computational domain is schematically shown in figure 9. A uniform supersonic flow with a given Mach number is imposed on the left boundary, while a supersonic outflow condition is set on the right boundary. Upper and lower boundaries are treated as non-reflecting interfaces, while a slip condition is imposed on the wedge surface. During each series of computations, the upper wedge angle is fixed, while the lower wedge angle is slowly varied to approximate the rotation around the leading edge. The previously converged flow is taken as the initial condition, as the geometry parameters vary. The numerical flow field is considered converged to a steady state when the positions of all the shock waves remain unchanged within a certain number of iterations. However, the Kelvin–Helmholtz slip layers (see Rikanati *et al.* 2006), which are unsteady in nature, can be captured in some cases for an overall MR configuration. Fortunately, this unsteadiness occurs in the supersonic region of the converging–diverging stream tube bounded by the slipstreams. It is neglected in the

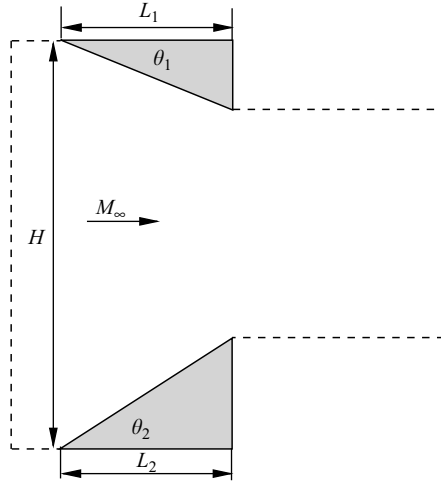


FIGURE 9. Schematic illustration of the computational domain.

convergence criteria, as it has an insignificant influence on the position of the MR wave configuration.

3.1. Curved RR wave patterns

As shown in figure 4, there is no intersection between the shock polars of both reflected shock waves in the graphical construction if the reflection occurs above the detachment condition and below the maximum-deflection condition. For an ideal reflection of shock waves, this leads to an overall MR solution. On the other hand, an overall RR wave pattern followed by a subsonic flow pocket is admissible for a reflection configuration with curved shock waves. The wave patterns are not steady but may be pseudo-steady (see Henderson 1990; Henderson & Menikoff 1998). In the reflection of shock waves induced by two asymmetrically posed wedges, the Prandtl–Meyer expansion fans following the reflection point help to provide sufficient boundary conditions for a steady overall RR with curved shock waves or strong solutions. A series of computations is conducted for a flow with $M_\infty = 5.04$. The angle of the upper wedge is kept constant at $\theta_1 = 22.42^\circ$ and $L_1 = L_2 = 0.55H$ (as shown in figure 9). Several important wedge angles associated with this series of computations are $\theta_1^{sym} = 27.7^\circ$, $\theta_2^S = 31.2^\circ$, $\theta_2^D = 31.8^\circ$ and $\theta_2^{MD} = 32.3^\circ$. The variation sequence of θ_2 is $\theta_2 = 30^\circ \rightarrow 31.5^\circ \rightarrow 32^\circ \rightarrow 32.3^\circ \rightarrow 32.6^\circ \rightarrow 32.3^\circ \rightarrow 31.5^\circ$.

The sequential wave patterns shown in figure 10 start from $\theta_2 = 30^\circ$ at which angle an overall RR with both straight reflected shock waves in the vicinity of the reflection point was achieved. The wave configuration is an oRR (wRR + wRR) type with a completely supersonic flow behind the two reflected shock waves (figure 10a, b). When θ_2 is increased to $\theta_2 = 32.3^\circ = \theta_2^{MD} > \theta_2^D = 31.8^\circ$, the overall RR is maintained as shown in figure 10(c). However, the oRR features the curvature of reflected shock waves followed by a subsonic flow pocket as shown in figure 10(d). This wave structure has also been illustrated by Li *et al.* (1999) under the detachment condition and was denoted as oRR (wRR + sRR). At $\theta_2 = 32.6^\circ > \theta_2^{MD}$, an RR can no longer exist and changes to an overall MR wave configuration, as shown in figure 10(e, f).

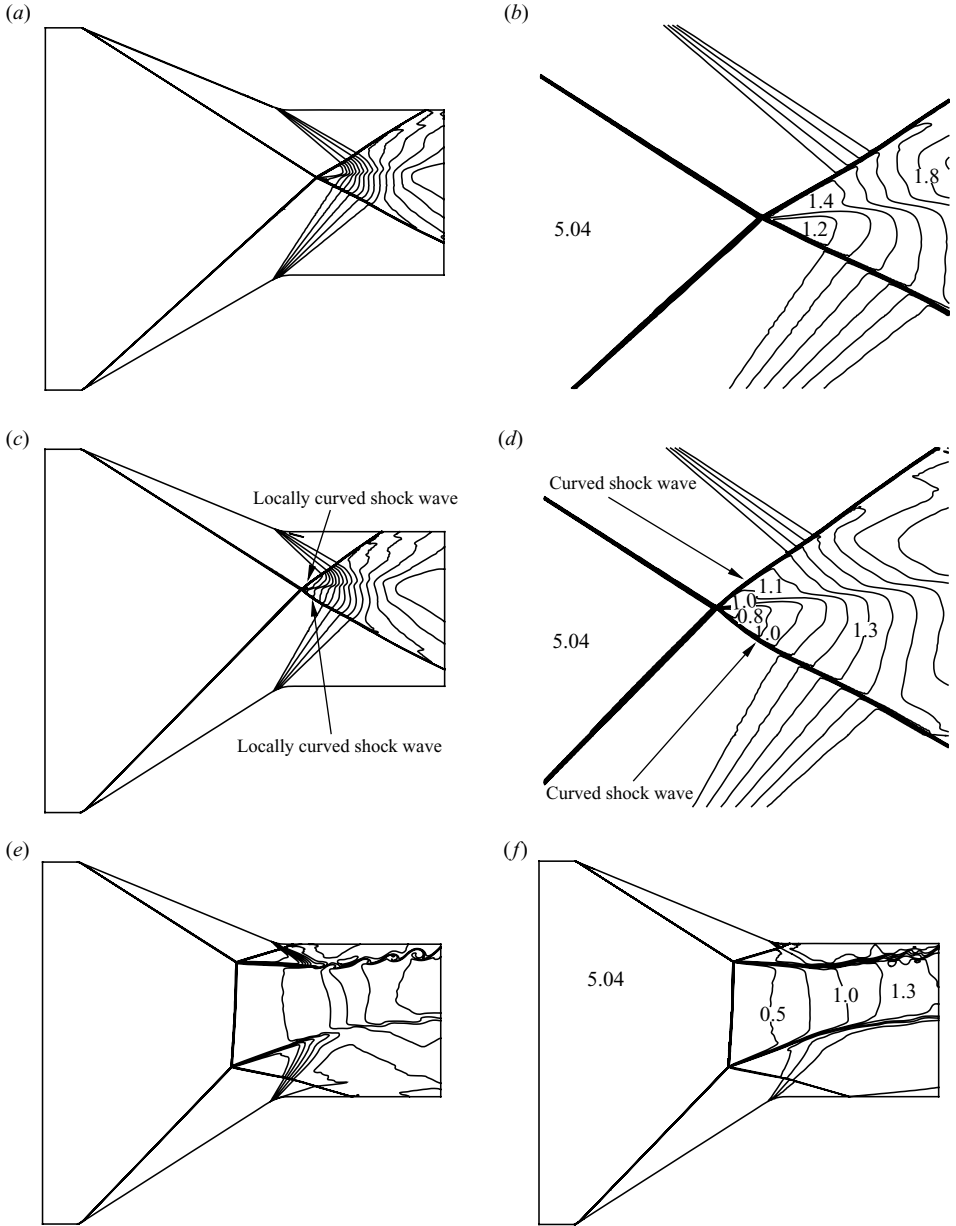


FIGURE 10. Numerical contours of density (left) and Mach number (right), illustrating the reflection wave configuration: (a, b) overall RR with both straight shock waves when $\theta_2 = 30^\circ$; (c, d) overall RR with curved shock waves when $\theta_2 = 32.3^\circ$; (e, f) overall MR when $\theta_2 = 32.6^\circ$; ($M_\infty = 5.04$, $\theta_1 = 22.42^\circ$, $L_1 = L_2 = 0.55H$, mesh nodes 801×801).

Three more computations for $\theta_2 = 32.3^\circ$ on different grids with 1001×1001 , 1201×1201 , 1601×1601 mesh nodes reach an identical oRR solution with a locally curved wave structure as shown in figure 11 by Mach number contours. This implies that the oRR wave configuration at θ_2^{MD} , which is theoretically impossible, cannot be ascribed to the numerical viscosity.

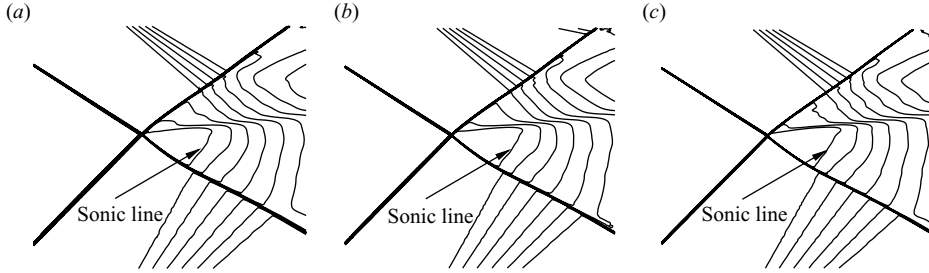


FIGURE 11. Numerical contours of Mach number illustrating grid independence; Mesh point (a) 1001×1001 ; (b) 1201×1201 ; (c) 1601×1601 ($M_\infty = 5.04$, $L_1 = L_2 = 0.55H$, $\theta_1 = 22.42^\circ$, $\theta_2 = 32.3^\circ$).

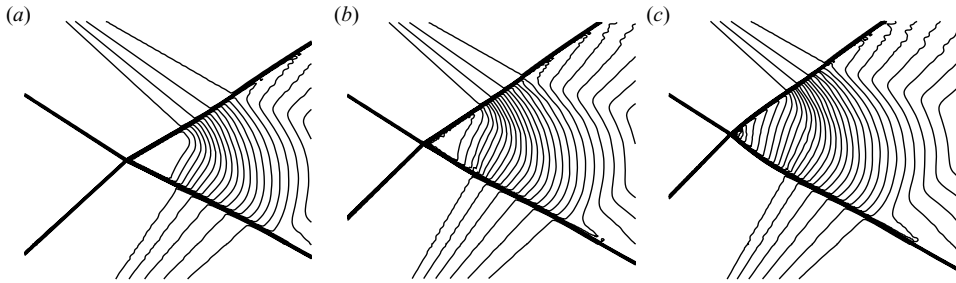


FIGURE 12. Numerical contours of pressure illustrating the smooth variation of pressure and curved shock wave structure: (a) $\theta_2 = 30.0^\circ$; (b) $\theta_2 = 31.5^\circ$; (c) $\theta_2 = 32.3^\circ$ ($M_\infty = 5.04$, $L_1 = L_2 = 0.55H$, $\theta_1 = 22.42^\circ$, mesh nodes 801×801).

Figure 12 shows the pressure contours in the near field about the interaction point for $\theta_2 = 30.0^\circ$, $\theta_2 = 31.5^\circ$, $\theta_2 = 32.3^\circ$. Differences can be found in the region bounded by the reflected shock waves and the first characteristic of the expansion waves. In figure 12(a), where $\theta_2 < \theta_2^S$, the region is completely supersonic with straight reflected shock waves and a uniform pressure field which can be theoretically predicted by the intersection of shock polars. When θ_2 slightly exceeds θ_2^S , as shown in figure 12(b), the lower reflected shock becomes slightly curved. If θ_2 further increases to θ_2^{MD} , as shown in figure 12(c), the pressure in the flow region smoothly varies between two pressure ratios corresponding to the maximum-deflection conditions of the $(p-\theta)$ loci for both reflected shock waves. It can be confirmed from these computations that the curved shock segment along with the smooth change of pressure makes an oRR wave structure possible at $\theta_2^D \leq \theta_2 \leq \theta_2^{MD}$. Besides the three-dimensional effects, which likely contaminate the results as mentioned by the authors, the curved wave structures can be an additional explanation for the experimental transition angle beyond theoretical value as shown in figure 9 of Li *et al.* (1999).

3.2. Effects of the expansion fans

A series of computations is conducted to evaluate the effects of the location of the expansion fans. The upstream effects of the expansion fans on the reflection can be weakened by increasing the wedge lengths. The upper and lower wedge angles are 22.4° and 32.3° , respectively. The sonic line in the oRR wave configuration moves downstream following the expansion fans, as shown in figure 13(a, b), where $L_1 = L_2 = 0.5H$ and $L_1 = L_2 = 0.55H$, respectively. Setting the wedge lengths to $0.6H$ triggers an RR \rightarrow MR transition, as illustrated by figure 13(c). However, the reflected

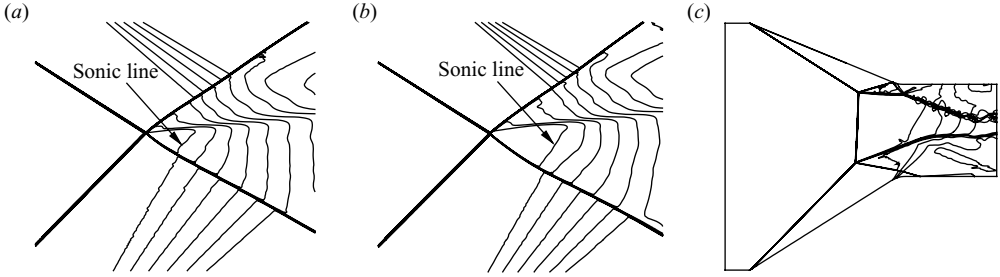


FIGURE 13. Numerical contours of flow Mach number illustrating the effects of the location of expansion fans: (a) $L_1 = L_2 = 0.5H$; (b) $L_1 = L_2 = 0.55H$; (c) $L_1 = L_2 = 0.60H$ ($M_\infty = 5.04$, $\theta_1 = 22.42^\circ$, $\theta_2 = 32.3^\circ$, mesh nodes 1601×1601).

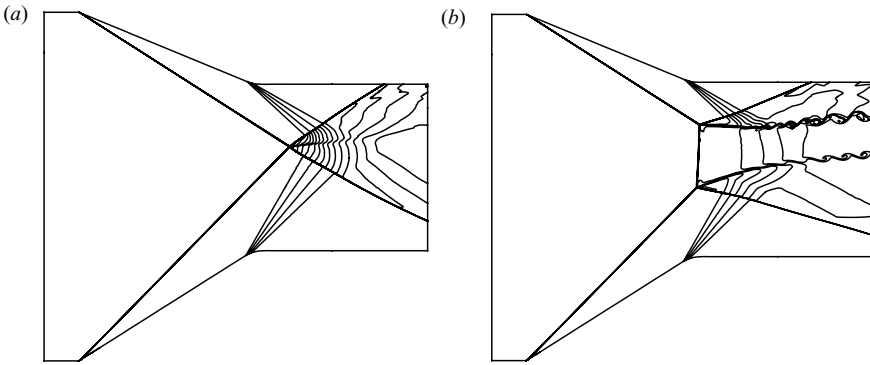


FIGURE 14. Numerical contours of density illustrating the effects of transient movement of the expansion fans on the RR \rightarrow MR transition: (a) overall RR when $L_1 = L_2 = 0.5H$; (b) overall MR when L_1 and L_2 are decreased from $0.5H$ to $0.475H$ ($M_\infty = 5.04$, $\theta_1 = 22.42^\circ$, $\theta_2 = 32.3^\circ$, mesh nodes 1601×1601).

shock wave r_1 (see notation in figure 1) reaches and is reflected from the upper wedge surface. The re-reflected shock wave interacts with the slipstream s_1 , which results in a series of disturbance propagating upstream in the subsonic flow domain. Here, figure 13(c) presents a transient oMR wave pattern, as the inviscid simulation doesn't provide enough dissipative mechanism against the disturbance. These different solutions shown in figure 13(a–c) can lead to the conclusion that the upstream effects of the expansion waves delay the RR \rightarrow MR transition.

The location of the expansion fans affects the transition condition. In addition, the transient movement of the expansion fans also plays a role. Here, the transient movement of the expansion fans is approximated by artificial change of the wedge lengths. The oRR wave configuration is shown by density contours in figure 14(a) for $\theta_1 = 22.42^\circ$, $\theta_2 = 32.3^\circ$ and $L_1 = L_2 = 0.5H$. Using this solution as the initial condition and slightly decreasing the wedge lengths from $0.5H$ to $0.475H$, a sequential computation reaches an oMR solution as shown in figure 14(b). Further computations indicate that RR \rightarrow MR transition cannot be realized by transiently changing the wedge lengths if θ_2 is less than θ_2^S . This coincides with the experimental study of Li *et al.* (1999) in which the data scatter inside $(\theta_2^S, \theta_2^{MD})$ for an upper wedge angle $\theta_1 = 22^\circ$. According to figure 8, the threshold for an RR \rightarrow MR transition about this wedge angle is large enough to bear relatively intensive disturbance.

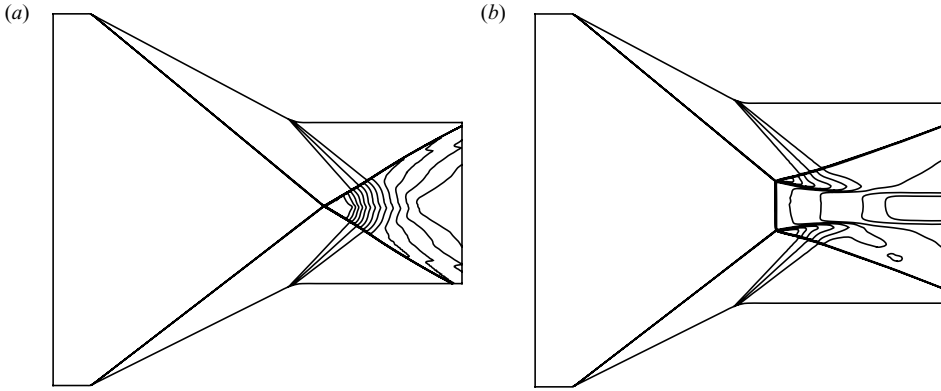


FIGURE 15. Numerical contours of density illustrating the reflection wave configuration: (a) overall RR when $L_1 = L_2 = 0.55H$; (b) overall MR when L_1 and L_2 are decreased to $0.45H$; ($M_\infty = 5.04$, $\theta_1 = 28^\circ$, $\theta_2 = 26.5^\circ$, mesh nodes 801×801).

3.3. Asymmetry vs symmetry

In the following series of simulations, the upper wedge angle is $\theta_1 = 28^\circ$, which is very close to the symmetry angle $\theta_1^{sym} = 27.7^\circ$, and the lower wedge angle is $\theta_2 = 26.5^\circ$. The critical angles associated with different RR → MR transition criteria are $\theta_2^S = 27.5^\circ$ and $\theta_2^T \approx \theta_2^{MD} = 27.65^\circ$. As illustrated in figure 8, the threshold of the RR → MR transition is relatively small under the present flow and geometry conditions.

The computation when $L_1 = L_2 = 0.55H$ is undoubtedly converged at the weak solution of shock wave reflection according to the shock polar analysis. The oRR wave pattern is shown in figure 15(a) by density contours. After the wedge lengths are reduced to $0.5H$, the overall RR wave configuration can be maintained. A further reduction of the wedge lengths to $0.45H$ triggers the RR → MR transition, as shown in figure 15(b). It should be noted that the fluid flow shown in figure 15(a) is completely supersonic, and both reflected shock waves are straight in the vicinity of the reflection point. In other words, the numerical disturbance generated by the transient movement of the expansion waves is strong enough to trigger an RR → MR transition. Here, the lower wedge angle is lower than the sonic-point and the detachment criteria.

It can be concluded from above computational results that an additional cause for the earlier RR → MR transition reported by Sudani *et al.* (2002) may be the disturbance generated by the transient movement of the expansion fans. In their experimental set-up, the upper wedge was varied in both the vertical and horizontal directions, which should accordingly cause a movement of the expansion fan, emanating from the trailing edge of the wedge. The second important aspect is that the wedge arrangements in the experiments are relatively close to the corresponding symmetric reflection condition. An earlier RR → MR transition was also reported by Chpoun *et al.* (1995) in their experiments concerning hysteresis in the reflection of symmetric shock waves. Moreover, the free stream flow Mach number of the test facility used by Sudani *et al.* (2002), a blowdown-type wind tunnel, is small compared to that of the SH2 wind tunnel used by Li *et al.* (1999), which may be the third critical aspect. Considering the threshold for the RR → MR transition and the effects of the expansion waves, it is not surprising that the good agreement reported by Li *et al.* (1999) and the disagreement reported by Sudani *et al.* (2002) between experimental and theoretical results are both reasonable.

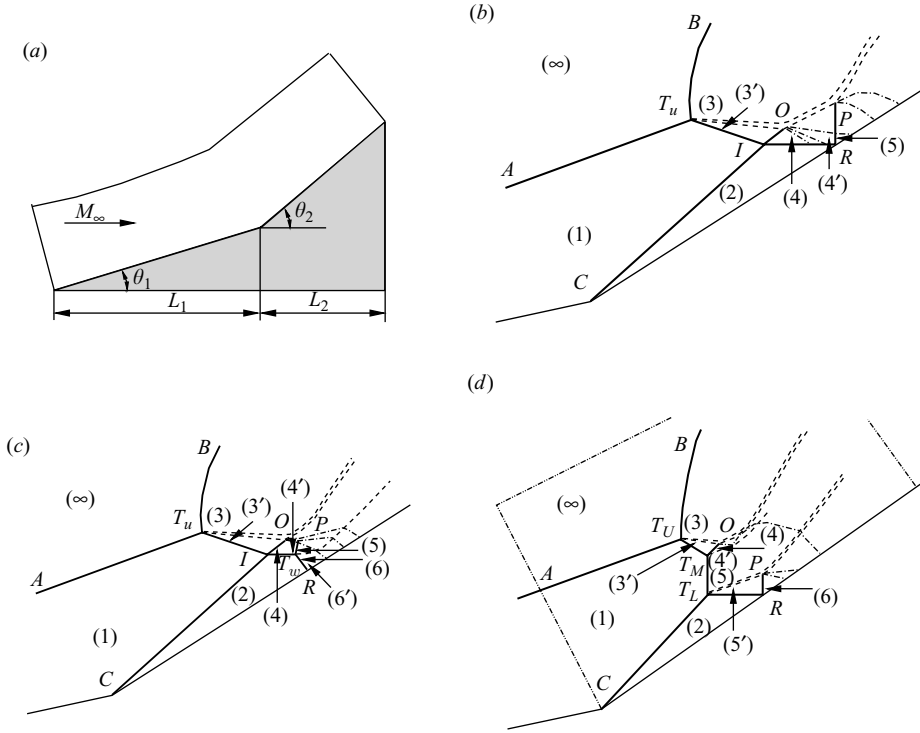


FIGURE 16. Schematic illustration of shock wave patterns in the interactions of shock waves on double-wedge-like geometries: (a) double-wedge-like geometries; (b), (c) and (d) three types of wave patterns associated with the interaction of shock waves of opposite families at distinct wedge differences, $\Delta\theta = \theta_2 - \theta_1$ (Solid line: shock wave; dashed line: slipstream; dashed-dotted line: expansion wave).

3.4. Advanced RR \rightarrow MR transition caused by a transverse wave

Shock/shock interactions on double-wedge-like geometries, as shown in figure 16(a), in a hypersonic flow are considered a fundamental research problem related to hypersonic flights. Edney (1968) used shock polar diagrams and classified the interactions of oblique shock waves and bow shocks on a cylinder. Through his experimental research, it was realized that abnormally high heating and pressure loads can be induced by shock/shock interactions on hypersonic vehicles and that a small variation in the geometry can lead to a major change in the overall flow structure. Olejniczak, Wright & Candler (1997) numerically studied shock interactions and their transition on double-wedge-like geometries. Recently, Ben-Dor *et al.* (2003) revealed that hysteresis and self-induced oscillations exist in the shock flow pattern for various angles of inclination of the second wedge.

A Type V (following Edney's taxonomy) wave configuration occurring within a certain scope of $\Delta\theta$ can be further divided into three subclasses, as shown in figures 16(b–d). In the first case, the leading shock wave (CI) emanating from the leading edge of the second wedge and the shock wave ($T_U I$) originating from the upper triple point T_U undergo an overall RR. Moreover, one of the reflected shock waves, IR, is re-reflected from the second wedge surface in a regular type. In the second case, an MR occurs over the second wedge surface instead of the RR in the previous case, while the RR wave pattern at point 'I' is maintained. In contrast, an

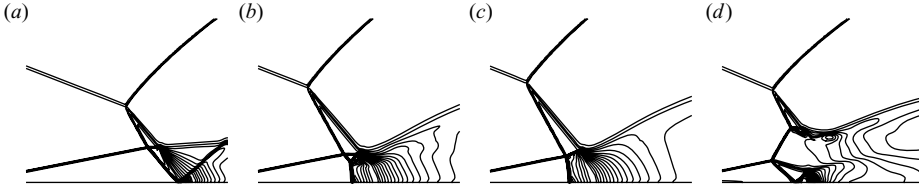


FIGURE 17. Density contour illustrating numerical solutions for the shock/shock interactions on double-wedge-like geometries: (a) $\Delta\theta = 26.2^\circ$ with a regular reflection of shock waves $T_U I$ and $C I$; (b) $\Delta\theta = 26.65^\circ$; (c) $\Delta\theta = 27.1^\circ$; (d) $\Delta\theta = 28.3^\circ$ with a Mach-type reflection of shock waves $T_U T_M$ and $C T_L$ ($M_\infty = 9$, $\theta_1 = 15^\circ$).

overall MR occurs when $\Delta\theta$ is increased slightly in the last case. In this subsection, the mechanism that advances the RR → MR transition is numerically investigated.

The flow domain is shown in figure 16(a). The shock wave interaction phenomena depend on the relevant parameters which are, under the inviscid flow hypothesis, the free stream Mach number M_∞ , the ratio of the specific heats γ , the first wedge length L_1 and the wedge angles θ_1 and θ_2 or alternatively the difference between the two wedge angles, $\Delta\theta = \theta_2 - \theta_1$. In the following simulations, γ is 1.4 for a perfect diatomic gas, $L_1 = 5$ cm, $M_\infty = 9$ and $\theta_1 = 15^\circ$, while θ_2 or $\Delta\theta$ varies continuously for different cases. Under these conditions, the flow Mach number behind the first leading shock is 5.04, which is identical to the free stream flow Mach number for the cases illustrated in former subsections. The computational domain is defined by the rectangular region bounded by the dashed-dotted lines, as shown in figure 16(d), and is turned around the second wedge corner in a clockwise direction by an angle of θ_2 . The inflow conditions for the free stream flow and the flow behind the first leading shock, AT_U , can be specified by oblique shock wave relations.

The wave configurations for the shock/shock interactions over the second wedge surface are shown in figure 17(a–d), and the shock polar solutions are given in figure 18(a–c). All of the $\Delta\theta$ angles are in the dual-solution domain according to shock polar analysis. At $\Delta\theta = 26.2^\circ$, as shown in figure 16(b) and figure 17(a), the reflection of shock waves $T_U I$ and $C I$ as well as that of shock wave IR over the wedge surface are both regular. In this case, the flow deflection angles and pressure increases in flow regions (1), (2), (3, 3') and (4) (figure 16b) can also be theoretically defined. However, due to the effects of a series of expansion waves emanating from point O , the flow conditions in regions (4') and (5) cannot be directly obtained from the shock polar solution. The reflection of IR changes to a Mach-type reflection, as shown in figure 17(b), when $\Delta\theta$ is increased to 26.65° . In this case, the flow deflection angles and pressure ratios in all of the labelled regions in figure 16(c) can be determined on the shock polars, as shown in figure 18(a). At a critical angle of $\Delta\theta = 27.1^\circ$, the triple-point T_W and the reflection point I , as well as the shock waves IO and $T_W P$, coincide, as shown in figure 17(c). This is also the strong solution labelled by (6) in figure 18(b). According to the shock entropy theorem, this solution is generally unstable. However, the above-mentioned wave pattern can be maintained here due to the converge–diverge stream tube which is formed between the slipstream and the wedge surface. A further increase in $\Delta\theta$ leads to an RR → MR transition, as shown in figures 17(d) and 18(c) and in the schematics of figure 16(d).

Thus, the RR → MR transition angle $\Delta\theta = 27.2^\circ$ is smaller than the corresponding detachment criterion $\theta_2^D = 31.8^\circ$. Here, the shock wave $T_W P$ plays an important role as a trigger for the advanced transition. It is also interesting to note that within the

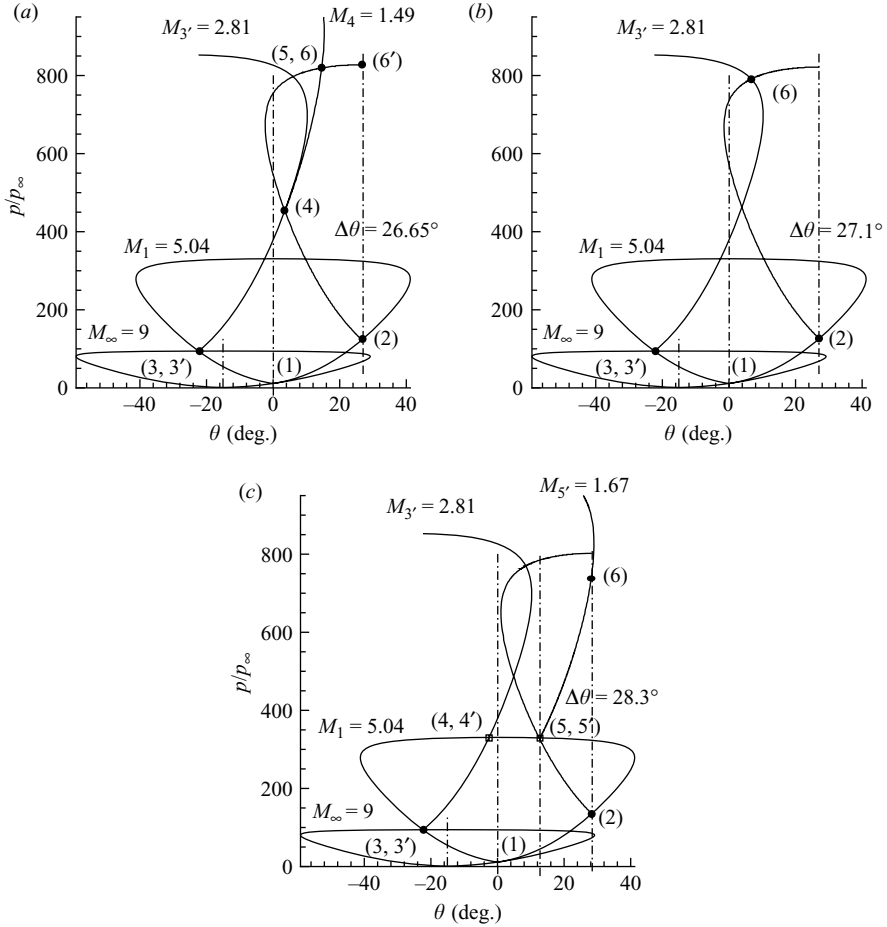


FIGURE 18. Shock polar solutions for the shock/shock interactions on double-wedge-like geometries: (a) $\Delta\theta = 26.65^\circ$; (b) $\Delta\theta = 27.1^\circ$; (c) $\Delta\theta = 28.3^\circ$ ($M_\infty = 9$, $\theta_1 = 15^\circ$).

small scope of the wedge angle difference of $27.2^\circ \leq \Delta\theta \leq 28^\circ$, the wave configuration undergoes a periodic oscillation among all wave patterns given in figure 17. Ben-Dor *et al.* (2003) revealed that oscillation of the shock wave patterns is associated with the interaction of shock waves and slipstreams emanating from the triple-points. Consequently, the second wedge surface is exposed to oscillating aerodynamic forces and heating loads.

4. Conclusions

The RR \rightarrow MR transition is analytically and numerically studied for the reflection of asymmetric shock waves in steady flows. The RR \rightarrow MR transition can occur between the sonic-point and maximum-deflection conditions in which the location and transient movement of the expansion waves, which are inherent flow structures, play an important role. Based on these two critical conditions and the threshold for the RR \rightarrow MR transition, it has been found that both the good agreement and the disagreement between experimental and theoretical results found in previous studies

are realistic consequences of the nature underlying the reflection of asymmetric shock waves.

Two-dimensional inviscid computations verify an overall RR with locally curved wave structures and smooth change of pressure at the maximum-deflection angle. It is also found that an RR \rightarrow MR transition can be triggered by the rapid movement of the trailing edge. Moreover, in the vicinity of the symmetric reflection condition, the movement of expansion fans is more effective due to the relatively small threshold for the RR \rightarrow MR transition compared to that in an asymmetric reflection condition. Numerical results also indicate that the RR \rightarrow MR transition can be advanced by a transverse wave from the downstream flow field in the shock/shock interaction on a double-wedge-like geometry in a steady hypersonic flow.

The RR \rightarrow MR transition process and the hysteresis phenomenon have a significant impact on the performance of the supersonic intake of an air-breathing propulsion scheme. Therefore, the present RR \rightarrow MR transition analysis is useful for a better understanding of the physics associated with the reflection of asymmetric shock waves as well as for the intake flow of a supersonic/hypersonic air-breathing propulsion system.

The authors thank Professor A. Chatterjee from Research Center for Aircraft Parts Technology in Gyeongsang National University for polishing the English text and the constructive discussions. The authors also thank Dr Y. L. Gao and C. Wang from LHD Laboratory in the Institute of Mechanics in Beijing for their constructive discussions and suggestions. This work was supported by the Korea Research Foundation under grant no. KRF-2005-005-J09901.

REFERENCES

- BEN-DOR, G. 1991 *Shock Wave Reflection Phenomena*. Springer.
- BEN-DOR, G. 2006 A state-of-the-knowledge review on pseudo-steady shock-wave reflections and their transition criteria. *Shock Waves* **15**, 277–294.
- BEN-DOR, G., ELPERIN, T., LI, H. & VASILEV, E. I. 1999 The influence of downstream-pressure on the shock wave reflection phenomenon in steady flows. *J. Fluid Mech.* **386**, 213–232.
- BEN-DOR, G., IVANOV, M., VASILEV, E. I. & ELPERIN, T. 2002 Hysteresis processes in the regular reflection \leftrightarrow Mach reflection transition in steady flows. *Prog. Aerosp. Sci.* **38** (4), 347–387.
- BEN-DOR, G., VASILEV, E. I., ELPERIN, T. & ZENOVICH, A. V. 2003 Self-induced oscillations in the shock wave flow pattern formed in a stationary supersonic flow over a double wedge. *Phys. Fluids* **15** (12), L85–L88.
- CHPOUN, A. & BEN-DOR, G. 1995 Numerical confirmation of the hysteresis phenomenon in the regular to the Mach reflection transition in steady flows. *Shock Waves* **5**, 199–203.
- CHPOUN, A., PASSEREL, D., LI, H. & BEN-DOR, G. 1995 Reconsideration of oblique shock wave reflections in steady flows. Part 1. Experimental investigation. *J. Fluid Mech.* **301**, 19–35.
- EDNEY, B. 1968 Anomalous heat transfer and pressure distributions on blunt bodies at hypersonic speeds in the presence of an impinging shock. *Tech Rep.* 115. The Aerospace Research Institute of Sweden.
- HAN, Z. & YIN, X. 1993 *Shock Dynamics*. Kluwer.
- HENDERSON, L. F. 1990 The von Neumann paradox for the diffraction of weak shock waves. *J. Fluid Mech.* **213**, 71–94.
- HENDERSON, L. F., COLELLA, P. & PUCKETT, E. G. 1991 On the refraction of shock waves at a slow-fast gas interface. *J. Fluid Mech.* **224**, 1–27.
- HENDERSON, L. F., CRUTCHFIELD, W. Y. & VIRGONA, R. J. 1997 The effect of heat conductivity and viscosity of argon on shock waves diffracting over rigid ramps. *J. Fluid Mech.* **331**, 1–36.
- HENDERSON, L. F. & MENIKOFF, R. 1998 Triple shock entropy theorem and its consequences. *J. Fluid Mech.* **366**, 179–210.

- HORNUNG, H. G. 1997 On the stability of steady-flow regular and Mach reflection. *Shock Waves* **7**, 123–125.
- HORNUNG, H. G., OERTEL, H. & SANDEMAN, R. J. 1979 Transitions to Mach reflection of shock waves in steady and pseudo-steady flow with and without relaxation. *J. Fluid Mech.* **90**, 541–560.
- IVANOV, M., ZEITOUN, D., VUILLON, J., GIMELSHEIN, S. & MARKELOV, G. 1996 Investigation of the hysteresis phenomena in steady shock reflection using kinetic and continuum methods. *Shock Waves* **5**, 341–346.
- IVANOV, M. S., BEN-DOR, G., KUDRYAVTSEV, A. N. & KHOTYYANOVSKY, D. V. 2002 The reflection of asymmetric shock waves in steady flows: a numerical investigation. *J. Fluid Mech.* **469**, 71–87.
- IVANOV, M. S., MARKELOV, G. N., KUDRYAVTSEV, A. N. & GIMELSHEIN, S. F. 1998 Numerical analysis of shock wave reflection transition in steady flows. *AIAA J.* **36** (11), 2079–2086.
- IVANOV, M. S., VANDROMME, D., FOMIN, V. M., KUDRYAVTSEV, A. N., HADJADI, A. & KHOTYANOVSKY, D. V. 2001 Transition between regular and Mach reflection of shock waves: new numerical and experimental results. *Shock Waves* **11**, 199–207.
- JIANG, Z. L., TAKAYAMA, K. & CHEN, Y. S. 1995 Dispersion conditions for non-oscillatory shock-capturing schemes and its applications. *Comput. Fluid Dyn. J.* **2**, 137–150.
- JIANG, Z. L. 2004 On the dispersion-controlled principles for non-oscillatory shock-capturing schemes. *Acta Mech. Sinica* **20** (1), 1–15.
- KUDRYAVTSEV, A. N., KHOTYANOVSKY, D. V., IVANOV, M. S., HADJADI, A. & VANDROMME, D. 2002 Numerical investigation of transition between regular and Mach reflections caused by free-stream disturbances. *Shock Waves* **12**, 157–165.
- LI, H. & BEN-DOR, G. 1996 Application of the principle of minimum entropy production to shock wave reflection. Part I. Steady flow. *J. App. Phys.* **80**, 2027–2037.
- LI, H., CHPOUN, A. & BEN-DOR, G. 1999 Analytical and experimental investigations of the reflection of asymmetric shock waves in steady flows. *J. Fluid Mech.* **390**, 25–43.
- MOUTON, C. & HORNUNG, H. G. Experimental investigation of tripping between regular and Mach reflection in the dual-solution domain. In *26th Intl Symp. on Shock Waves*, Göttingen, Germany.
- NAIDOO, K. & SKEWS, B. W. Computational and experimental investigation of dynamic shock reflection phenomena. In *26th Intl Symp. on Shock Waves*, Göttingen, Germany.
- VON NEUMANN, J. 1943 Refraction, interaction and reflection of shock waves. *Tech Rep.* vol. 203–245. NAVORD.
- OLEJNICZAK, J., WRIGHT, W. J. & CANDLER, G. V. 1997 Numerical study of inviscid shock interactions on double-wedge geometries. *J. Fluid Mech.* **352**, 1–25.
- RIKANATI, A., SADOT, O., BEN-DOR, G., SHVARTS, D., KURIBAYASHI, T. & TAKAYAMA, K. 2006 Shock-wave Mach-reflection slip-stream instability: a secondary small-scale turbulent mixing phenomenon. *Phys. Rev. Lett.* **96** (17), 4503:1–4503:4.
- SKEWS, B. W. 1997 Aspect ratio effects in wind tunnel studies of shock wave reflection transition. *Shock Waves* **7**, 373–383.
- SKEWS, B. W. 2000 Three-dimensional effects in wind tunnel studies of shock wave reflection. *J. Fluid Mech.* **407**, 85–104.
- SUDANI, N. & HORNUNG, H. G. 1998 Stability and analogy of shock wave reflection in steady flow. *Shock Waves* **8**, 367–374.
- SUDANI, N., SATO, M., KARASAWA, T., NODA, J., TATE, A. & WATANABE, M. 2002 Irregular effects on the transition from regular to Mach reflection of shock waves in wind tunnel flows. *J. Fluid Mech.* **459**, 167–185.
- VUILLON, J., ZEITOUN, D. & BEN-DOR, G. 1995 Reconsideration of oblique shock wave reflections in steady flows. Part 2. Numerical investigation. *J. Fluid Mech.* **301**, 37–50.